

# Segregation Phenomena in Size-selected Bimetallic CuNi Nanoparticle Catalysts

*Lukas Pielsticker<sup>†</sup>, Ioannis Zegkinoglou<sup>†</sup>, Nuria J. Divins<sup>†</sup>, Hemma Mistry<sup>‡</sup>, Yen-Ting Chen<sup>†</sup>,  
Aleksander Kostka<sup>†</sup>, Jorge Anibal Boscoboinik<sup>#</sup>, and Beatriz Roldán Cuenya<sup>†◊,\*</sup>*

<sup>†</sup> Department of Physics, Ruhr University Bochum, 44780 Bochum, Germany

<sup>‡</sup> Department of Physics, University of Central Florida, Orlando, Florida 32816, United States

<sup>†</sup>Zentrum für Grenzflächendominierte Höchstleistungswerkstoffe (ZGH), Ruhr University Bochum, 44780 Bochum, Germany

<sup>#</sup>Center for Functional Nanomaterials, Brookhaven National Laboratory, Upton, New York 11973-5000, United States

<sup>◊</sup>Department of Interface Science, Fritz-Haber Institute of the Max Planck Society, Berlin 14195, Germany

\*Roldan@fhi-berlin.mpg.de

This document is the unedited Author's version of a Submitted Work that was subsequently accepted for publication in J. Phys. Chem B, copyright © American Chemical Society after peer review. To access the final edited and published work see <https://pubs.acs.org/doi/10.1021/acs.jpcc.7b06984>.

## ABSTRACT

Surface segregation, restructuring and sintering phenomena in size-selected copper-nickel nanoparticles (NPs) supported on silicon dioxide substrates were systematically investigated as a function of temperature, chemical state and reactive gas environment. Using near-ambient pressure (NAP-XPS) and ultra-high vacuum X-ray photoelectron spectroscopy (XPS), we showed that nickel tends to segregate to the surface of the NPs at elevated temperatures in oxygen- or hydrogen-containing atmospheres. It was found that the NP pre-treatment, gaseous environment and oxide formation free energy are the main driving forces of the restructuring and segregation trends observed, overshadowing the role of the surface free energy. The depth profile of the elemental composition of the particles was determined under *operando* CO<sub>2</sub> hydrogenation conditions by varying the energy of the X-ray beam. The temperature dependence of the chemical state of the two metals was systematically studied, revealing the high stability of nickel oxides on the NPs and the important role of high valence oxidation states in the segregation behavior. Atomic force microscopy (AFM) studies revealed a remarkable stability of the NPs against sintering at temperatures as high as 700 °C. The results provide new insights into the complex interplay of the various factors which affect alloy formation and segregation phenomena in bimetallic NP systems, often in ways different from those previously known for their bulk counterparts. This leads to new routes for tuning the surface composition of nanocatalysts, for example through plasma and annealing pre-treatments.

## INTRODUCTION

Catalytic systems based on bimetallic alloy nanoparticles (NPs) often exhibit significantly superior catalytic properties compared to their monometallic counterparts as a result of synergetic geometrical and electronic effects between the constituent metals.<sup>1-10</sup> Segregation phenomena may take place during the chemical reaction and modify the elemental composition of the surface, crucially affecting the catalytic activity and selectivity of the system towards certain products. In bulk metal alloys, phase segregation is a result of the complex interplay of a number of factors, which include the atomic radii of the metals,<sup>11-12</sup> their surface free energy,<sup>13</sup> the oxide formation enthalpy,<sup>14-15</sup> and the metals' affinity to form stable chemical bonds with adsorbate species.<sup>16-19</sup> With the exception of the atomic radii, all other factors can differ significantly in NPs compared to bulk systems, often as a function of the particle size, leading to distinct surface properties. Understanding the way in which surface chemical and morphological restructuring affects the catalytic properties of the NPs under reaction conditions is important for further optimizing the efficiency of such systems.

Copper-nickel (CuNi) alloys have been successfully employed as catalysts in a number of reactions, including carbon dioxide and carbon monoxide hydrogenation,<sup>20-24</sup> hydrogenolysis of ethane and propane,<sup>25-26</sup> the reverse water-gas-shift reaction,<sup>27</sup> ethanol steam reforming<sup>28-29</sup> and methane decomposition,<sup>30</sup> exhibiting increased catalytic activity compared to their monometallic counterparts. Doping of Cu surfaces with Ni has been theoretically shown to strongly promote methanol synthesis.<sup>31-33</sup> The addition of CO into the CO<sub>2</sub> hydrogenation reaction mixture further promotes methanol synthesis, an observation which was partly attributed to CO-induced surface segregation of Ni.<sup>34</sup> Given that the atomic radii of Cu and Ni are very similar (128 pm versus

124 pm),<sup>35</sup> the size misfit does not play an important role with respect to segregation in this system. In reduced chemical state and in the absence of surface adsorbates, Cu is expected to segregate towards the surface of the particles due to its lower surface free energy.<sup>14, 36-37</sup> In the presence of oxides or oxygen-containing adsorbates, the situation is much more complex. In bulk bimetallic systems, the Gibbs free energy for NiO is higher (less negative) than that of CuO, but lower than that of Cu<sub>2</sub>O.<sup>15, 38</sup> This means that in bulk CuNi alloys, the segregation trends for Cu<sup>+</sup> and Cu<sup>2+</sup> are in principle opposite to each other, with Cu<sup>2+</sup> preferentially segregating to the surface and Cu<sup>+</sup> inwards. Different preparation conditions and chemical states of the metals can thus lead to different segregation trends in the presence of oxygen.<sup>39-42</sup>

Little is known about the restructuring in CuNi NPs. It was shown that Cu<sub>2</sub>O is much more stable in NPs than in bulk and that the stability of both Cu oxides is strongly dependent on the particle size.<sup>43</sup> Furthermore, Ni<sup>3+</sup> species in oxide compounds, which are usually unstable in bulk materials, seems to be more stable in NPs.<sup>44</sup> NAP-XPS studies on CuNi NPs recently showed that Cu segregates to the surface upon annealing in O<sub>2</sub>,<sup>45</sup> contrary to what would be expected for bulk alloys based on the Gibbs free energy. It becomes obvious that it is very difficult to know in advance the segregation behavior of Cu and Ni in an oxidizing environment for a NP of a given size. In the presence of hydrogen-containing adsorbates, the stronger chemical bonds that hydrogen forms with nickel compared to copper are in principle expected to result in surface segregation of Ni.<sup>25, 46</sup> But also in this case the particle size affects the surface composition, given that smaller particles promote alloying of the metals (due to higher diffusion rates<sup>47</sup>) and alloy particles have decreased oxide reduction temperatures compared to segregated monometallic phases.<sup>48</sup> The chemical state is also crucial, because the presence of metal oxides in the as-prepared samples can actually reverse the trend expected based on the surface energies

and the adsorbate effect.<sup>49</sup> Finally, the interaction of the metals with the substrate is always of significant importance, since sintering, interdiffusion and chemical bonding may affect the morphology and the stoichiometry of the particles.<sup>50-53</sup>

In order to shed light on the interplay and relative importance of the various factors which affect the surface properties of bimetallic CuNi NPs, under conditions which are relevant for catalytic CO<sub>2</sub> hydrogenation, we have studied the morphological stability and chemical state of size-selected (~ 5 nm) Cu<sub>0.6</sub>Ni<sub>0.4</sub> NPs supported on SiO<sub>2</sub>/Si(111). Emphasis is given to the understanding of temperature- and adsorbate-induced alloying and segregation phenomena in reducing and oxidizing environments. The sample morphology was characterized via *ex situ* atomic force microscopy (AFM) before and after the annealing. The chemical surface composition of the bimetallic NPs was investigated via X-ray photoelectron spectroscopy (XPS) both using a monochromatic Al K<sub>α</sub> X-ray source in a UHV lab setup and at a synchrotron-based near-ambient pressure XPS (NAP-XPS) setup, where a depth profile of the particles was acquired by varying the photon energy under *operando* reaction conditions.

## EXPERIMENTAL

Size-selected bimetallic Cu<sub>0.6</sub>Ni<sub>0.4</sub> NPs with an average diameter of 5 nm were synthesized via inverse micelle encapsulation, a colloidal synthesis method which enables extensive control of the NP size and the interparticle distance.<sup>54-58</sup> Poly(styrene)-block-poly(2-vinylpyridine) (PS-P2VP) diblock copolymers (PS:P2VP ratio of 48500:70000, Polymer Source, Inc.) were dissolved in toluene to form micellar cages. The micelles were then loaded with copper(II)

nitrate hexahydrate ( $\text{Cu}(\text{NO}_3)_2 \cdot 6 \text{H}_2\text{O}$ ) and nickel(II) nitrate trihydrate ( $\text{Ni}(\text{NO}_3)_2 \cdot 3 \text{H}_2\text{O}$ ), leading to the formation of size-selected bimetallic CuNi NPs with narrow size distribution.

The micelle-encapsulated NPs were deposited on  $\text{SiO}_2/\text{Si}(111)$  substrates via dip-coating at a speed of 5 cm/min. The polymeric ligands were then removed by *ex situ*  $\text{O}_2$  plasma etching (SPI Plasma Prep III Plasma Etcher, 20 minutes, 20 W, 350 mTorr). For some of the samples, the dip-coating and plasma etching procedure was repeated multiple times to achieve higher coverage of the substrate with particles. Subsequently, the samples were loaded into an ultra-high vacuum (UHV) system (SPECS GmbH) where they were further treated with *in situ*  $\text{O}_2$  plasma (3 x 15 minutes, 9.8 W,  $3 \cdot 10^{-5}$  mbar) to remove adventitious carbon from sample transfer in air. The successful removal of the polymeric and adventitious carbon by the two plasma treatments is demonstrated by the lack of any C1s peak in high-resolution XPS spectra (see Supporting Information (SI), Figure S1).

After the *in situ*  $\text{O}_2$  plasma treatment, one sample (S1) was reduced by *in situ*  $\text{H}_2$  plasma (45 minutes, 8 W,  $3 \cdot 10^{-5}$  mbar) and then stepwise annealed in vacuum ( $10^{-9}$  mbar) in the UHV preparation chamber for 20 min in 150 °C steps (250 °C, 400 °C, 550 °C, 700 °C). A second, identically prepared sample (S2) was annealed in a high-pressure cell attached to the UHV system following the same temperature steps under a pressure of 1 bar  $\text{O}_2$ . After each annealing step, the samples were transferred in vacuum to an UHV analysis chamber, where XPS measurements were acquired using a monochromatic Al  $K_\alpha$  X-ray source ( $h\nu = 1486.7$  eV) and a hemispherical electron analyzer (Phoibos 150, SPECS GmbH). The pass energy of the electron analyzer was 15 eV.

In order to study the effect of gaseous adsorbates and in particular of a CO<sub>2</sub> / H<sub>2</sub> reaction mixture under *operando* conditions, identically prepared samples were investigated using NAP-XPS at beamline CSX-2 of the NSLS-II synchrotron at Brookhaven National Laboratory (USA). To increase the NP loading on the surface, in order to compensate for the attenuation of the electrons in the gaseous environments, these samples were dip-coated (and subsequently treated with *ex situ* O<sub>2</sub> plasma) three times. XPS spectra were acquired *in situ* in O<sub>2</sub> (0.2 Torr, 400 °C), in H<sub>2</sub> (0.5 Torr, 400 °C), in a CO<sub>2</sub> / H<sub>2</sub> reaction mixture (1:3 volume ratio, 0.68 Torr total pressure, at 210 °C and 240 °C), and in pure CO<sub>2</sub> (0.5 Torr, 240 °C). The measurements were performed at two different photon energies (1130 eV, 1540 eV) to obtain depth profile information of the near surface elemental composition. After each step, the sample was cooled down, the chamber was evacuated, and the new gas was introduced approximately at room temperature (RT).

For investigating the NP morphology and possible sintering, AFM images were acquired *ex situ* in tapping mode (Bruker MultiMode 8 AFM) before and after annealing. The size distribution of the NPs was obtained by measuring at least 150 individual NPs in each image using the open-source software *Gwyddion*.

## RESULTS & DISCUSSION

AFM images of two identically prepared Cu<sub>0.6</sub>Ni<sub>0.4</sub> NP samples supported on SiO<sub>2</sub>/Si(111) substrates are shown in Figure 1, both in their as-prepared state (after *ex situ* O<sub>2</sub> plasma) and after annealing in reducing (UHV) or in oxidizing (O<sub>2</sub>) environment. The freshly prepared

samples are characterized by an average particle size of  $(5.2 \pm 0.7)$  nm and a narrow particle size distribution. Representative height histograms are shown in Figure S2 of the SI. The particle sizes given in the histograms refer to their heights, as determined by AFM. The lateral resolution of AFM is lower due to the tip convolution effect. This can lead to apparent NP diameter differences in the AFM images. Given that the particles have a spherical shape (see also Scanning Transmission Electron Microscopy (STEM) images in Figures S3, S4 in SI), the lateral size of the particles is considered equal to their height. The spatial distribution of the NPs on the substrates is homogeneous. The morphology of the NPs does not change significantly upon annealing. The average interparticle distance remains the same, demonstrating the remarkable stability of the NPs against sintering, even upon high temperature (700 °C) heating in UHV (S1), as opposed to previous studies on Cu/SiO<sub>2</sub> NP systems.<sup>50</sup> This may be due to the initial O<sub>2</sub> plasma treatment leading to a strong oxidized-metal/oxide support interface. The average particle size was found to decrease to  $(3.0 \pm 0.4)$  nm after UHV annealing at 700 °C (S1) and to  $(2.1 \pm 0.4)$  nm upon O<sub>2</sub> annealing at the same temperature (S2). This can be at least partially attributed to the loss of metals via sublimation and/or to the interaction with the substrate. Such interaction might involve inward NP diffusion facilitated by a possible low-temperature SiO<sub>x</sub> decomposition catalyzed by the NPs or the growth of the SiO<sub>2</sub> layer in O<sub>2</sub> leading to a partial embedding of the NPs into the substrate and an apparent smaller NP height.<sup>52, 54-56</sup> The chemical reduction of the initially oxidized metals is unlikely to be responsible for the size decrease, firstly because the NPs probably re-oxidize during the AFM measurements (which are performed in air), and secondly because the chemical reduction can anyway only account for a size decrease of ~ 15% at most (see Table S1, SI). Similar observations are made for the samples investigated under *operando* reaction conditions with NAP-XPS, except that no significant decrease of the particle

size occurs in this case (possibly due to the lower temperatures employed for those measurements compared to the UHV studies and the absence of *in situ* O<sub>2</sub> plasma pre-treatment). No evidence of sintering is present on those samples either (see AFM images displayed in Figure S5, SI).

XPS spectra from the Cu 2p and Ni 2p core level regions acquired at RT in UHV ( $1 \cdot 10^{-9}$  mbar) after different plasma and annealing treatments are shown in Figure 2. The elemental Si 2p peak from the SiO<sub>2</sub>/Si support (at a binding energy of 99.4 eV)<sup>57</sup> was used for energy calibration in all spectra. The Cu 2p<sub>3/2</sub> (a) and Ni 2p<sub>3/2</sub> (b) regions were fitted with Gaussian-Lorentzian line-shapes (ratio 0.3) and a linear background. In agreement with the literature,<sup>58-61</sup> the Cu 2p<sub>3/2</sub> spectra were fitted with a single peak corresponding to metallic Cu<sup>0</sup> or Cu<sup>+</sup> (Cu<sub>2</sub>O) at 932.6 eV, two peaks for Cu<sup>2+</sup> (CuO) at 933.7 eV and 935.1 eV, and two peaks for shake-up satellite features at 942.4 eV and 944.7 eV. The energy difference between the Cu<sup>0</sup> and Cu<sup>+</sup> 2p<sub>3/2</sub> peaks ( $\sim 0.1$  eV) is too small to be experimentally resolved in lab-based XPS. Distinction between Cu<sup>0</sup> and Cu<sup>+</sup> with the help of the LMM Auger lines was not possible in this study due to the low count rates resulting from the small particle coverage. A Cu(OH)<sub>2</sub> component at 935.3 eV is also present after O<sub>2</sub> plasma (sample S2).<sup>62</sup> For the deconvolution of the Ni 2p<sub>3/2</sub> spectra a metallic component (853.1 eV) with an asymmetric line-shape was used in the fittings. The area ratio, the binding energy offset and the width of its two satellite features (at 856.8 eV and 859.1 eV) were constrained in the fittings following the work of Biesinger *et al.*<sup>63</sup> The binding energy of the Ni<sup>0</sup> component is  $\sim 0.5$  eV higher than reported in the literature and increases with increasing temperature due to a particle size effect.<sup>64-65</sup> The peak at binding energy around 856.7 eV can be attributed to either Ni(OH)<sub>2</sub> (Ni<sup>2+</sup>) or Ni<sub>2</sub>O<sub>3</sub> / NiOOH (Ni<sup>3+</sup>).<sup>63-64, 66-67</sup> Its satellite feature was

fitted with one component at 862.2 eV.  $\text{Ni}^{3+}$  oxides are generally unstable in bulk materials, but there have been indications that they are more stable on NPs.<sup>44</sup> For the sample annealed in  $\text{O}_2$ , a  $\text{Ni}^{2+}$  (NiO) component at 854.1 eV was also included.<sup>64, 68</sup> The binding energy shift as a result of the alloying of the two metals is expected to be only about 0.1 eV, which is below our experimental resolution.<sup>69-70</sup>

Initial *in situ* treatment with an  $\text{H}_2$  plasma, prior to the annealing in UHV (Figure 2, sample S1), results in a mostly reduced state of both metals. While the presence of  $\text{Cu}^+$  cannot be excluded, it is more likely that the peak around 932.6 eV in the Cu  $2p_{3/2}$  spectrum corresponds to  $\text{Cu}^0$ , because Ni oxides are in general more stable than Cu oxides and Ni is already mostly reduced after  $\text{H}_2$  plasma. The Ni spectra are dominated by the metallic  $\text{Ni}^0$  peak at 853.1 eV and its satellites, but a remaining contribution of  $\sim 15\%$  from  $\text{Ni}^{3+}$  or  $\text{Ni}(\text{OH})_2$  is still present after the  $\text{H}_2$  plasma. It is noted that a reduction of the Ni oxide only by annealing in UHV (700 °C for 20 minutes or 500 °C for 180 minutes), *i.e.* without the use of any  $\text{H}_2$  plasma or reducing gas environment, was not possible in our study. Such attempts resulted in the loss of Cu before the Ni oxide was reduced.

The initial *in situ*  $\text{O}_2$  plasma treatment of an identical sample (Figure 2, sample S2) results in a highly oxidized state for both metals. The Cu  $2p_{3/2}$  spectrum contains mostly  $\text{Cu}^{2+}$  species ( $\text{Cu}(\text{OH})_2$  and  $\text{CuO}$ ) and only a small contribution of  $\text{Cu}^+$ . The presence of  $\text{Cu}(\text{OH})_2$  is likely due to the increase in the content of  $\text{H}_2\text{O}$  in our UHV chamber during the  $\text{O}_2$  plasma treatment. Upon annealing in 1 bar  $\text{O}_2$ , the  $\text{Cu}(\text{OH})_2$  and  $\text{Cu}_2\text{O}$  peaks disappear and only  $\text{CuO}$  contributions (together with the corresponding satellite features) remain in the Cu spectra. The intensity of the Cu 2p signal is drastically decreased above 550 °C and completely disappears at 700 °C, mostly

due to inward segregation, as will be explained in the following. Ni is likely in the form of Ni<sup>3+</sup> species after the initial O<sub>2</sub> plasma, as either Ni<sub>2</sub>O<sub>3</sub> or NiOOH. The presence of Ni(OH)<sub>2</sub> cannot be excluded, but Ni<sup>3+</sup> species are more likely, because the same peak line-shape was observed under *operando* O<sub>2</sub> annealing conditions in the NAP-XPS studies, as will be explained later in the text (Fig. 3). Upon annealing in 1 bar O<sub>2</sub>, the Ni<sup>3+</sup> peak intensity gradually decreases above 400 °C, while the NiO contribution (at 854.1 eV) increases from 11% (among all Ni species) to 63% at 700 °C. A gradual increase of the binding energy of the Ni<sup>2+</sup> component with temperature (see Figure S6, SI) is attributed to the temperature-induced decrease of the particle size.

To gain insight into the depth profile of CuNi NPs *in situ* under different environments, synchrotron-based NAP-XPS spectra were acquired (Figure 3). The inelastic mean free path (IMFP) of the Cu 2p and Ni 2p electrons in the CuNi NPs for the two different X-ray photon energies that were used are summarized in Table S2 (SI). For both spectral regions the IMFP is approximately 0.6 nm at the low photon energy (1130 eV) and ~ 1.1 nm at the high photon energy (1540 eV). In O<sub>2</sub> at 400 °C (0.2 Torr) both metals are highly oxidized (Cu<sup>2+</sup>, Ni<sup>3+</sup>). The presence of Ni(OH)<sub>2</sub> cannot be excluded, however the absence of a significant hydrogen source in the chamber under NAP-XPS O<sub>2</sub> annealing conditions, as well as the different line-shape of the Ni 2p<sub>3/2</sub> peaks compared to those under *operando* H<sub>2</sub> annealing conditions (see next paragraph), indicate that Ni<sup>3+</sup> species are more likely during O<sub>2</sub> annealing.

After subsequent exposure to H<sub>2</sub> at 400 °C (0.5 Torr), the NPs are mostly reduced, with only a small (~ 10%) remaining Cu<sup>2+</sup> component and approximately 13% Ni(OH)<sub>2</sub> present at the surface. The assignment of the peak at 856.7 eV to Ni(OH)<sub>2</sub> is not definite, because Ni<sup>3+</sup> species may also be present, but the high amount of hydrogen in the chamber in this case and the line-shape (in particular the peak-to-satellite area ratio) make the presence of Ni(OH)<sub>2</sub> more likely.

Both the metallic ( $\text{Ni}^0$ ) and the  $\text{Ni}(\text{OH})_2$  components were fitted using constraints (area ratio, energy differences) based on the work of Biesinger *et al.*<sup>63</sup>

The NPs are almost completely reduced in the  $\text{CO}_2 / \text{H}_2$  reaction mixture under  $\text{CO}_2$  reduction reaction conditions (240 °C). No  $\text{Ni}^{3+}$  or  $\text{Ni}(\text{OH})_2$  species are detected on the surface. A small amount of  $\text{Cu}^{2+}$  (~ 10%) may still be present. Upon annealing in pure  $\text{CO}_2$  at the same temperature, Ni becomes partly oxidized at the surface of the particles (Fig. 3b), but a significant amount of metallic  $\text{Cu}^0$  (42%) and  $\text{Ni}^0$  (22%) components remain as well.

The elemental composition determined from the integrated areas of the fitted curves after consideration of the corresponding sensitivity factors is summarized for the various samples discussed above in Figures 4 (UHV XPS) and 5 (NAP-XPS). The Cu to Ni ratio (Cu:Ni) decreases significantly with increasing temperature in all samples, independent of the chemical state and the adsorbate environment. The change is particularly drastic at temperatures above 400 °C, reaching in UHV a final value of 19 : 81 at 700°C (sample S1, Fig. 4a). In  $\text{O}_2$  the effect is even more prominent, since Cu disappears completely from the probing volume of the NPs at 700 °C, leaving only Ni behind (sample S2, Fig. 4b). To interpret these results one needs to consider two things: the phase segregation and surface restructuring of the particles, and the non-reversible loss of metal as a result of sublimation and/or inward NP diffusion into the  $\text{SiO}_2$  substrate. For the latter, the ratio of the metals to silicon, as determined from the XPS fittings, was determined (Figure S8, SI). It becomes obvious from the temperature dependence in Fig. S8 that both metal contents decrease upon heating, but the loss of Cu is larger than that of Ni. Cross-sectional STEM/EDS (Figure S4) does not indicate significant diffusion of metals into the substrate upon annealing, so the metal loss is most likely due to sublimation of highly mobile Cu. Thus, although the decrease of the Cu:Ni ratio observed in Figure 4 indicates surface segregation

of Ni at elevated temperatures, the conclusion cannot be definite due to the simultaneous non-reversible loss of copper, which contributes to the effect.

The depth profiles extracted from the NAP-XPS measurements shown in Figure 5, in combination with the corresponding metal-to-silicon ratios in Figure S9 (SI), give further insight into this question. The atomic ratio plots clearly demonstrate that in an O<sub>2</sub> atmosphere at 400 °C, the amount of Cu in the near-surface region of the particles (probed by the lower photon energy, 1130 eV) is lower than deeper inside the NPs. The opposite is the case for Ni, which exhibits about 10% higher atomic percentage close to the surface compared to deeper atomic layers. This result shows that Ni segregates to the surface in the presence of O<sub>2</sub>. This is in agreement with what would be expected for bulk materials containing Cu<sup>+</sup> and Ni<sup>2+</sup>, where surface segregation of Ni occurs according to the Ellingham diagram,<sup>15, 38</sup> but is different from the segregation trend previously observed in 11 nm large CuNi NPs, where copper comes to the surface of the NPs upon annealing in O<sub>2</sub> at 350°C.<sup>45</sup> The discrepancy underlines the complex interplay of the various factors affecting the segregation phenomena in NP systems, as discussed in the Introduction. The different chemical state of the metals in the two studies, and in particular the different ratio of Cu<sup>2+</sup> to Cu<sup>+</sup> and of Ni<sup>3+</sup> to Ni<sup>2+</sup> in the as-prepared samples, is most likely the main reason for the opposite segregation trend. Due to the initial O<sub>2</sub> plasma treatment of our samples (necessary for the polymer removal), the as-prepared chemical state is much more oxidized, resulting in Cu<sup>2+</sup> and Ni<sup>3+</sup> being the dominant species upon O<sub>2</sub> annealing in the NAP-XPS studies. In the study by Beaumont *et al.*, on the contrary, copper is only partly oxidized after the O<sub>2</sub> annealing treatment and nickel remains mostly metallic.<sup>45</sup> The Ni surface segregation in our NPs indicates that the oxide (or oxyhydroxide) formation Gibbs free energy for Ni<sup>3+</sup> is

smaller than for  $\text{Cu}^{2+}$ . To the best of our knowledge, such a calculated energy value (i.e., an Ellingham diagram for NPs) is not available. It is worth noting that the larger particle size in Beaumont *et al.* compared to our work may also be a factor contributing to the different segregation trends, given the dependence of the oxide formation enthalpy and the stability of metal oxides on this parameter.

The surface segregation of Ni becomes stronger upon reducing the NPs in  $\text{H}_2$  (0.5 Torr) at 400 °C. The difference of the atomic percentages between the near-surface and subsurface layers (Fig. 5) becomes higher (~ 15%) than in  $\text{O}_2$ , with more Ni being again present at the surface than in the interior of the NPs, and with the opposite trend observed for Cu. This behavior is consistent with previous segregation studies both in bulk and on NPs and can be attributed to the stronger chemical bonds formed between Ni and hydrogen adsorbates as compared to Cu.<sup>25, 46</sup> Although the presence of  $\text{Ni}(\text{OH})_2$  species in the NAP-XPS *operando* studies in  $\text{H}_2$  may also contribute to the observed segregation trend, the fact that the metal ratio (Fig. 5) remains practically the same in the subsequent  $\text{CO}_2 / \text{H}_2$  reaction mixture (where Ni is completely metallic), indicates that this contribution is not significant. Interestingly, surface segregation of Ni was also observed already at room temperature on the sample which was reduced with  $\text{H}_2$  plasma and then investigated in vacuum by XPS at the Al  $K_\alpha$  source (sample S1, Figure 4a). Based on the lower surface free energy of Cu compared to Ni, segregation of Cu to the surface should be expected.<sup>14</sup> The fact that the opposite trend is observed is due to the presence of hydrogen adsorbates at the surface of the NPs, which overshadows the free energy induced trend. It would be interesting to confirm the surface segregation of Cu in a fully reduced sample without the use of any adsorbates (i.e., no plasma and no annealing in gas), but this has not been possible in our study, because the nickel oxides are very stable in UHV even at the highest

temperatures we could reach (700 °C), and no metallic state could be achieved without losing the (more volatile) Cu species. A reduced Ni state could be only achieved with the help of H<sub>2</sub> plasma or annealing in H<sub>2</sub>, but then the adsorbate effect dominates the segregation behavior.

The surface segregation of Ni under CO<sub>2</sub> reaction conditions in the CO<sub>2</sub> / H<sub>2</sub> reaction mixture (Figure 5) is important for the interpretation of catalytic activity and selectivity results, given that Ni doping of Cu(111) surfaces is theoretically predicted to be beneficial for methanol synthesis from CO<sub>2</sub> hydrogenation, leading to the highest methanol yield among various other metal doping options (Au/Cu(111) < Cu(111) < Pd/Cu(111) < Rh/Cu(111) < Pt/Cu(111) < Ni/Cu(111)).<sup>31</sup> It is also relevant for the understanding of the promoting effect of adding CO to the CO<sub>2</sub> / H<sub>2</sub> reaction mixture.<sup>34</sup> In the former example, surface segregation of Ni was reported to take place in the presence of CO, which was found to be beneficial for methanol synthesis.<sup>34</sup> Our results demonstrate that, at least for the NP treatment that we applied, the desired surface segregation of Ni is achieved without the presence of CO in the reaction mixture. It is plausible that the initial O<sub>2</sub> plasma treatment of the CuNi NPs, followed by the H<sub>2</sub> annealing, is beneficial for the surface segregation of Ni through the creation of the highly oxidized Cu<sup>2+</sup> and Ni<sup>3+</sup> states. Further investigation on this is necessary.

The final step of the NAP-XPS study involved heating the CuNi sample in pure CO<sub>2</sub> (0.5 torr) at the same temperature as that of the CO<sub>2</sub> hydrogenation (240 °C). The segregation trend of the two metals is partly inverted under these conditions, with the percentage of Cu at the surface increasing and that of Ni decreasing. The result is a relatively mixed state, with no significant variation of the elemental stoichiometry with increasing depth. The depth profiles of the elemental composition of the NPs under the various annealing conditions discussed above are graphically visualized using three-dimensional atomic models, shown as insets in Figure 5. The

atomic ratios in the models correspond to the ratios determined by NAP-XPS. It is interesting that, although both O<sub>2</sub> and CO<sub>2</sub> are oxidizing gases, the segregation trends observed for these two gases are not the same. This demonstrates again the important role of the sample pre-treatment and the highly oxidized states produced upon O<sub>2</sub> plasma, which were present before any of the other annealing treatments in different gaseous environments were applied. Due to the fact that the oxide formation free energy lines for Cu<sup>+</sup>, Cu<sup>2+</sup>, Ni<sup>2+</sup> and Ni<sup>3+</sup> are entangled and intersect each other, the relative initial content of the different chemical states is crucial for the understanding of surface segregation. While a moderately oxidized state (like in pure CO<sub>2</sub> in our study or in O<sub>2</sub> in Beaumont *et al.*<sup>45</sup>) results in Cu surface segregation, the opposite may be the case when fully oxidized high-valence states are present.

## CONCLUSIONS

By using UHV and near-ambient pressure XPS, in combination with AFM, we were able to demonstrate the important role of surface adsorbates and the initial metal chemical state on the segregation phenomena of ~ 5 nm large size-selected CuNi NPs. By determining the atomic percentage of the two metals as a function of temperature and depth from the surface in different gas environments (UHV or *operando* in O<sub>2</sub>, H<sub>2</sub>, CO<sub>2</sub> / H<sub>2</sub> mixture, CO<sub>2</sub>), we could demonstrate that Ni segregates to the surface of the particles in O<sub>2</sub> when the metals are fully oxidized and high valence oxidation states are present. The surface segregation of Ni is further promoted upon annealing in H<sub>2</sub> and subsequently in a CO<sub>2</sub> hydrogenation reaction mixture (CO<sub>2</sub> : H<sub>2</sub> ratio 1:3) under *operando* conditions due to the adsorbate effect, which overshadows the role of the surface free energy. The presence of Ni at the surface of Cu-based catalysts is known to be beneficial for

obtaining high methanol yield. The NPs exhibit remarkable stability against sintering even at high temperatures (700 °C) in reducing environment, possibly because of the strongly oxidized substrate as a result of the initial O<sub>2</sub> plasma conditions. Treating the CuNi NPs with H<sub>2</sub> plasma prior to annealing in UHV also leads to the desired Ni surface segregation, already at room temperature. Our study sheds light on the complex interplay between the various factors which affect the surface morphology and chemical state of CuNi NPs and suggests that the surface atomic composition and thus the catalytic properties of the particles can be tuned by appropriate plasma and annealing treatments.

#### SUPPORTING INFORMATION

Details on XPS analysis; details on STEM/EDS characterization and FIB sample preparation; analysis histograms of NP heights from sample S1 and S2; AFM images before and after the NAP-XPS operando study; additional XPS analysis results; STEM images and EDS mapping; estimated decrease of particle size due to the reduction of monometallic Cu, Ni and bimetallic CuNi NPs; electron kinetic energies and inelastic mean free path for different X-ray excitation energies.

#### ACKNOWLEDGEMENT

We thank Dr. Mahdi Ahmadi for his help with the graphic design of the atomic models. This work was funded by the European Research Council (ERC-725915, OPERANDOCAT), and the German Federal Ministry of Education and Research (Bundesministerium für Bildung und Forschung, BMBF) under grant #03SF0523C –‘CO2EKAT’. Additional support was provided

by the US National Science Foundation (NSF- DMR-1207065). This research used resources of the Center for Functional Nanomaterials and the CSX-2 beamline of the National Synchrotron Light Source II, U.S. Department of Energy (DOE) Office of Science User Facilities operated for the DOE Office of Science by Brookhaven National Laboratory under Contract No. DE-SC0012704.

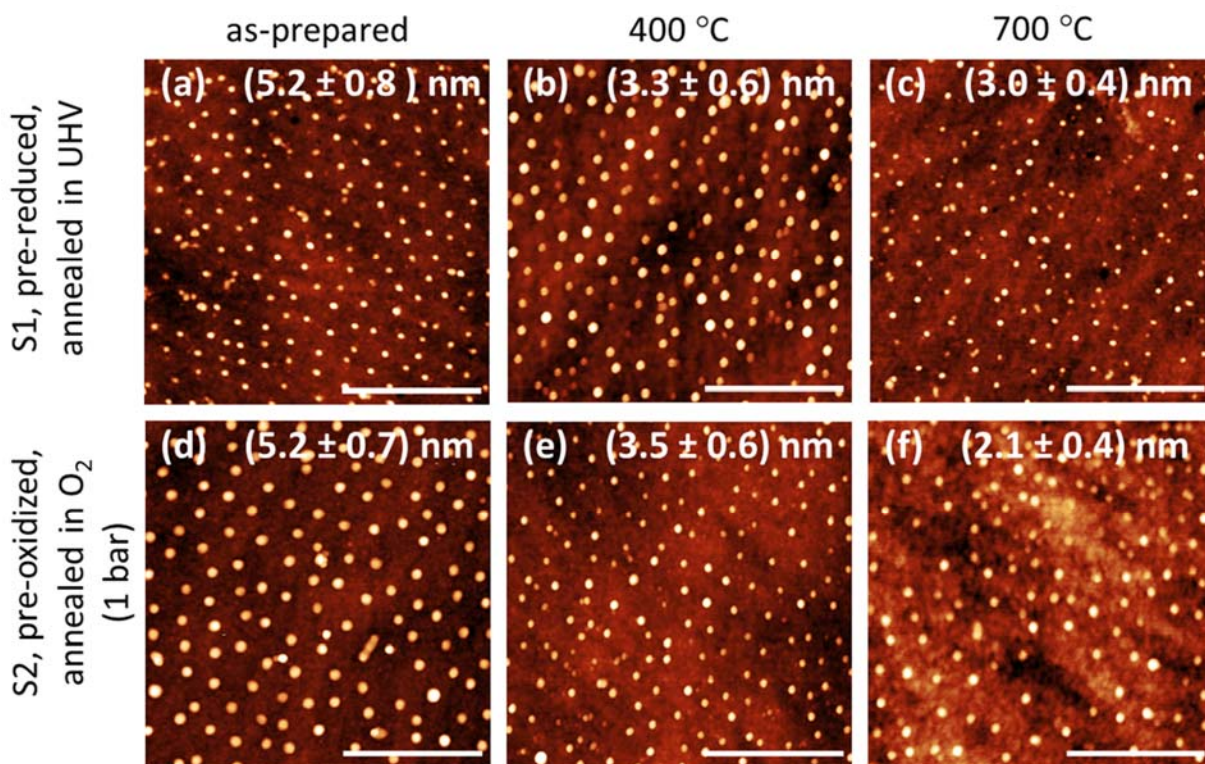


**Figure 1.** AFM images of size-selected ( $\sim 5$  nm) CuNi NPs supported on SiO<sub>2</sub>/Si(111) acquired at room temperature after the initial *ex situ* O<sub>2</sub> plasma treatment (a, d) and after annealing at the indicated temperatures. The annealing was performed in UHV for sample S1 (pre-reduced, b-c) and in 1 bar O<sub>2</sub> for sample S2 (pre-oxidized, e-f). All images display a 1 x 1  $\mu$ m sample region. The scale bar length is 400 nm.

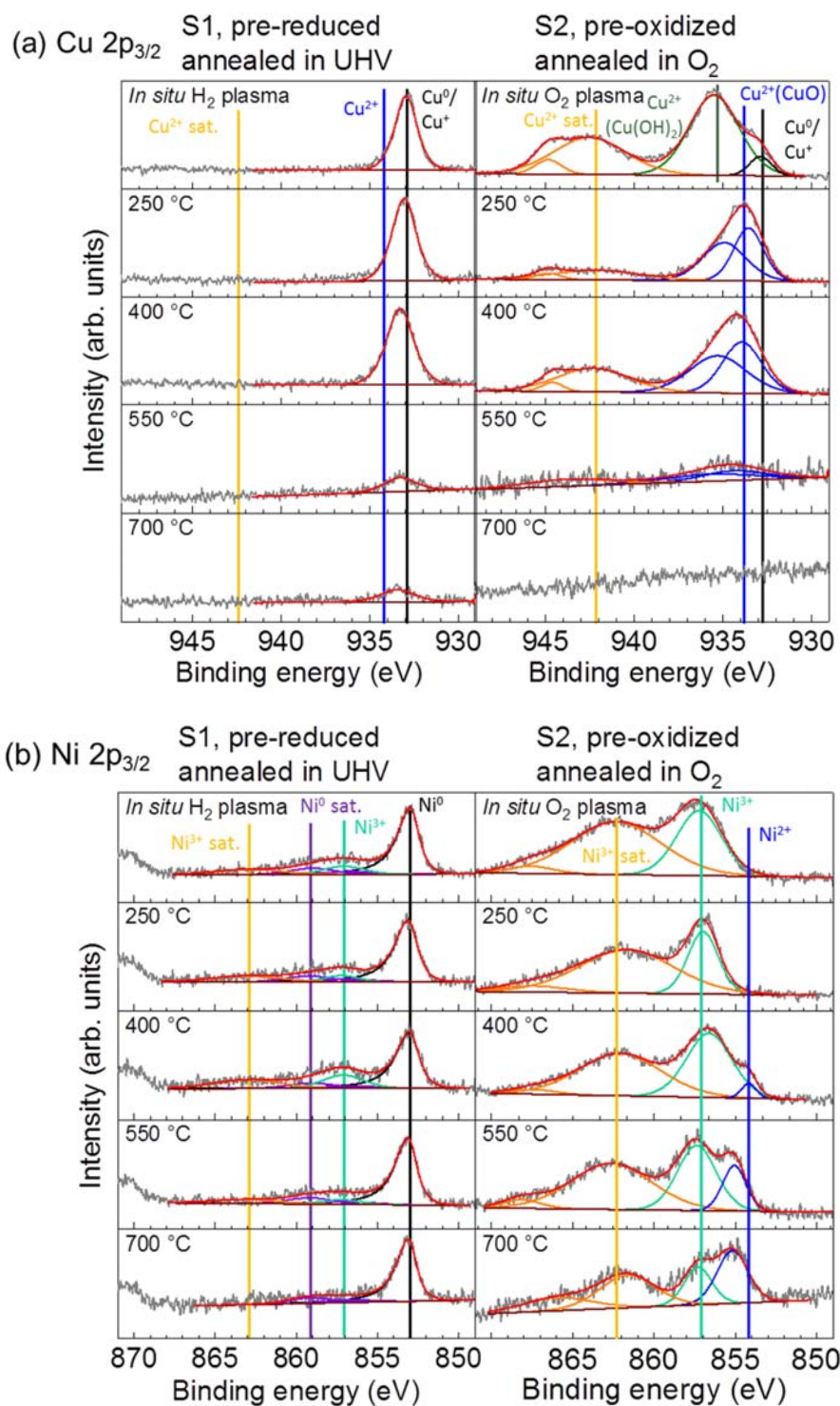


**Figure 2.** XPS spectra of the (a) Cu 2p<sub>3/2</sub> and (b) Ni 2p<sub>3/2</sub> core level regions of CuNi NPs on SiO<sub>2</sub>/Si(111) acquired at room temperature in UHV after different plasma and annealing treatments, as indicated on the graphs.

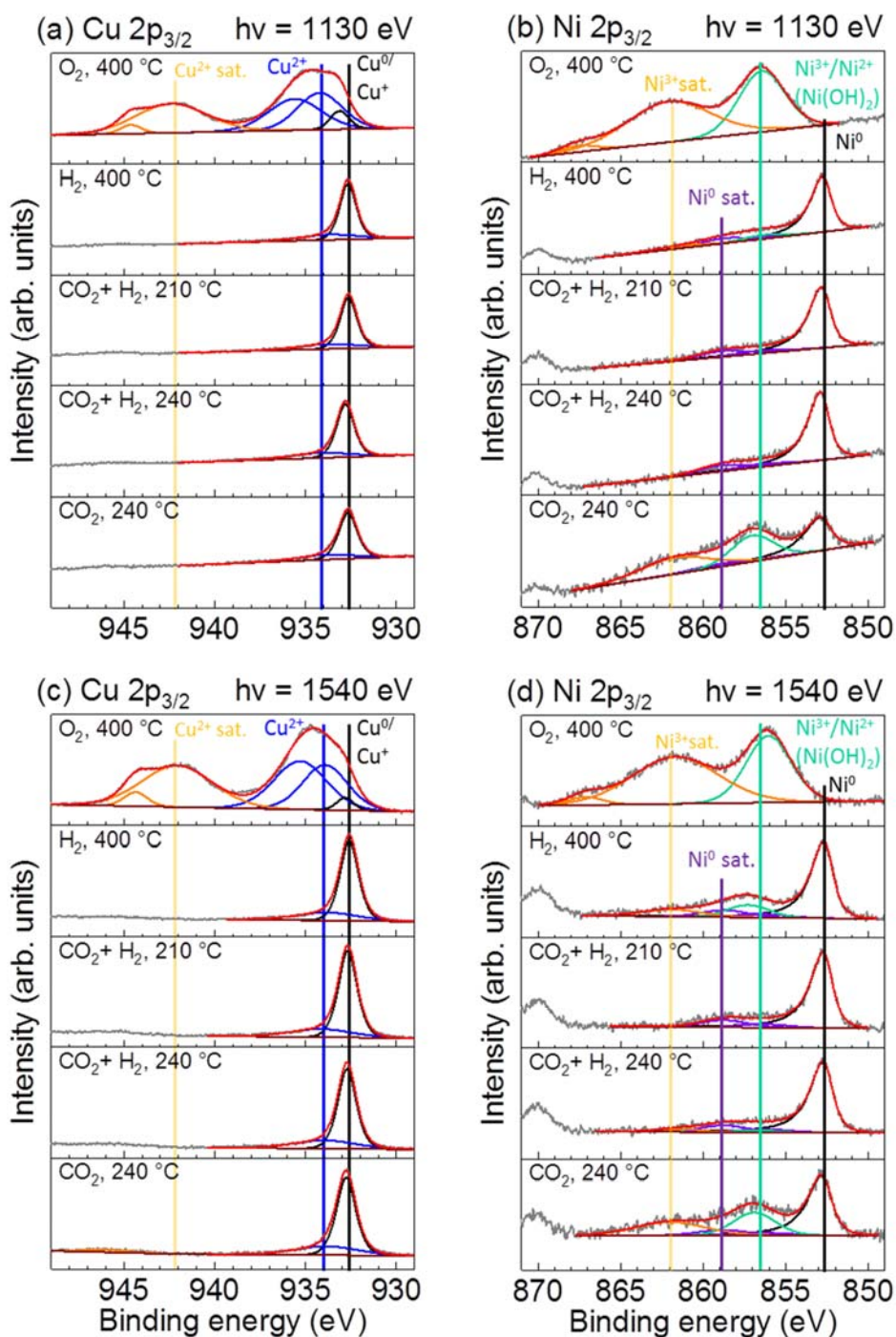


**Figure 3.** Near-ambient pressure XPS spectra of the Cu  $2p_{3/2}$  (a, c) and Ni  $2p_{3/2}$  (b, d) core level regions of CuNi NPs on  $\text{SiO}_2/\text{Si}(111)$  acquired *in situ* during annealing under various gas pressure and temperature conditions indicated on the graphs. X-ray photon energies of 1130 eV (a, b) and 1540 eV (c, d) were used for acquiring the depth profiles of the NPs.

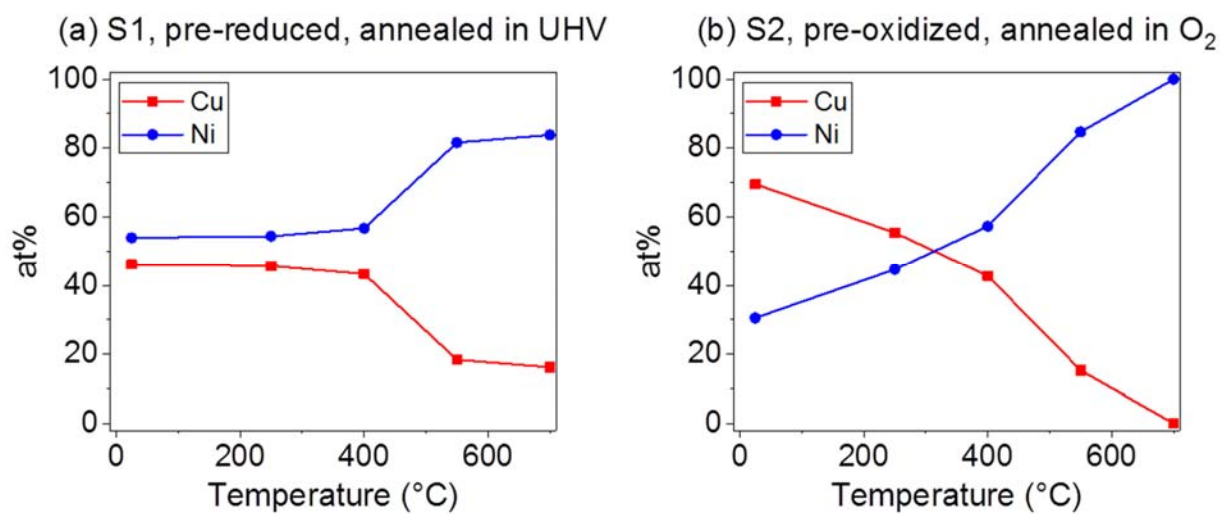


**Figure 4.** Cu and Ni atomic percentages as a function of annealing temperature, as determined with XPS measurements acquired in UHV at room temperature after annealing (a) in UHV (S1: pre-reduced sample) or (b) in 1 bar of O<sub>2</sub> (S2: pre-oxidized sample).

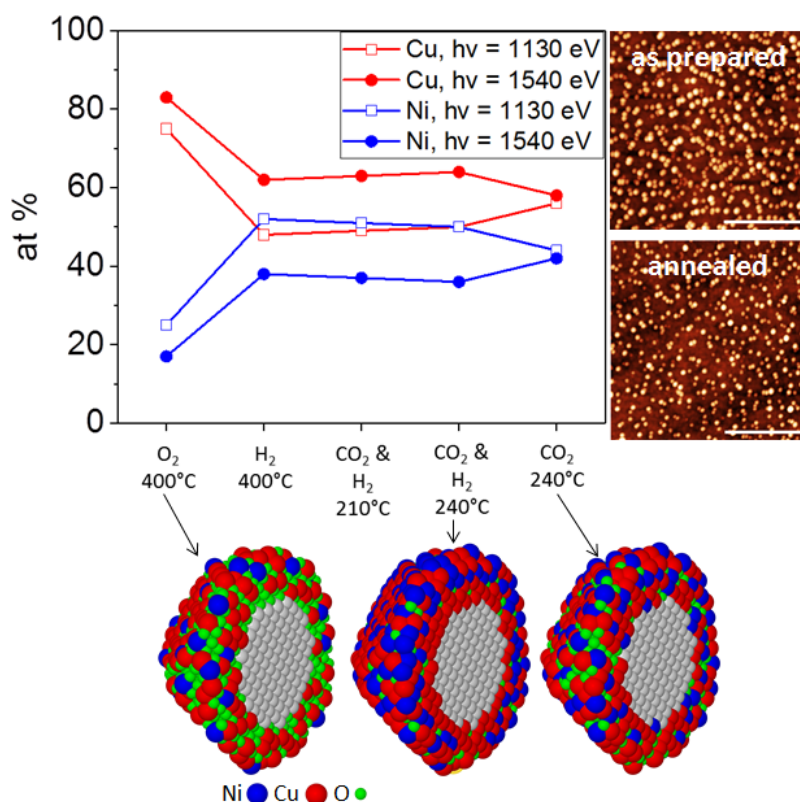


**Figure 5.** Cu (red) and Ni (blue) atomic percentages extracted from near-ambient pressure XPS measurements acquired *in situ* in the presence of various gases at the temperatures indicated on the graphs. The insets show AFM images of the sample before and after the annealing (scale bar: 400 nm), as well as atomic models of the NPs, where the variation of the elemental composition with the distance from the surface, as determined by NAP-XPS, is depicted. The grey area in the center depicts the volume of the NPs which is not probed within the sensitivity range of our XPS measurements (deeper than the IMFP). The model representations are for visual purposes only and do not reflect the actual crystallographic positions and sizes of the different atoms.

## REFERENCES

1. Cui, C.; Ahmadi, M.; Behafarid, F.; Gan, L.; Neumann, M.; Heggen, M.; Roldan Cuenya, B.; Strasser, P., Shape-Selected Bimetallic Nanoparticle Electrocatalysts: Evolution of Their Atomic-Scale Structure, Chemical Composition, and Electrochemical Reactivity under Various Chemical Environments. *Faraday Discuss.* **2013**, *162*, 91-112.
2. Liu, X.; Wang, D.; Li, Y., Synthesis and Catalytic Properties of Bimetallic Nanomaterials with Various Architectures. *Nano Today* **2012**, *7*, 448-466.
3. Sankar, M.; Dimitratos, N.; Miedzak, P. J.; Wells, P. P.; Kiely, C. J.; Hutchings, G. J., Designing Bimetallic Catalysts for a Green and Sustainable Future. *Chem. Soc. Rev.* **2012**, *41*, 8099-8139.
4. Singh, A. K.; Xu, Q., Synergistic Catalysis over Bimetallic Alloy Nanoparticles. *ChemCatChem* **2013**, *5*, 652-676.
5. Mistry, H.; Reske, R.; Strasser, P.; Roldan Cuenya, B., Size-Dependent Reactivity of Gold-Copper Bimetallic Nanoparticles During CO<sub>2</sub> Electroreduction. *Catal. Today* **2016**.
6. Chung, Y.-H.; Chung, D. Y.; Jung, N.; Park, H. Y.; Yoo, S. J.; Jang, J. H.; Sung, Y.-E., Origin of the Enhanced Electrocatalysis for Thermally Controlled Nanostructure of Bimetallic Nanoparticles. *J. Phys. Chem. C* **2014**, *118*, 9939-9945.
7. Kim, D.; Resasco, J.; Yu, Y.; Asiri, A. M.; Yang, P., Synergistic Geometric and Electronic Effects for Electrochemical Reduction of Carbon Dioxide Using Gold-Copper Bimetallic Nanoparticles. *Nat. Commun.* **2014**, *5*, 4948.
8. Shin, K.; Kim, D. H.; Lee, H. M., Catalytic Characteristics of AgCu Bimetallic Nanoparticles in the Oxygen Reduction Reaction. *ChemSusChem* **2013**, *6*, 1044-1049.
9. Yin, Z.; Zhou, W.; Gao, Y.; Ma, D.; Kiely, C. J.; Bao, X., Supported Pd-Cu Bimetallic Nanoparticles That Have High Activity for the Electrochemical Oxidation of Methanol. *Chem. Eur. J.* **2012**, *18*, 4887-4893.
10. Jimenez Divins, N.; Llorca, J., In Situ Photoelectron Spectroscopy Study of Ethanol Steam Reforming over RhPd Nanoparticles and RhPd/CeO<sub>2</sub>. *Appl. Catal., A* **2016**, *518*, 60-66.
11. Xin, H. L.; Alayoglu, S.; Tao, R.; Genc, A.; Wang, C.-M.; Kovarik, L.; Stach, E.A.; Wang, L.-W.; Salmeron, M.; Somorjai, G.A.; , Revealing the Atomic Restructuring of Pt-Co Nanoparticles. *Nano Lett.* **2014**, *14*, 3203-3207.
12. Wang, G.; van Hove, M. A.; Ross, P. N.; Baskes, M. I., Monte Carlo Simulations of Segregation in Pt-Ni Catalyst Nanoparticles. *J. Chem. Phys.* **2005**, *122*, 024706.
13. Liao, H.; Fisher, A.; Xu, Z. J., Surface Segregation in Bimetallic Nanoparticles: A Critical Issue in Electrocatalyst Engineering. *Small* **2015**, *11*, 3221-3246.
14. Ruban, A. V.; Skriver, H. L.; Nørskov, J. K., Surface Segregation Energies in Transition-Metal Alloys. *Phys. Rev. B* **1999**, *59*, 15990-16000.
15. Ellingham, H. J. T., Reducibility of Oxides and Sulphides in Metallurgical Processes. *Journal of the Society of Chemical Industry* **1944**, *63*, 125-160.
16. Lira, E.; Merte, L. R.; Behafarid, F.; Ono, L. K.; Zhang, L.; Roldan Cuenya, B., Role and Evolution of Nanoparticle Structure and Chemical State During the Oxidation of NO over Size- and Shape-Controlled Pt/ $\gamma$ -Al<sub>2</sub>O<sub>3</sub> Catalysts under Operando Conditions. *ACS Catal.* **2014**, *4*, 1875-1884.
17. Grass, M. E.; Park, M.; Aksoy, F.; Zhang, Y.; Kunz, M.; Liu, Z.; Mun, B. S., Effect of O<sub>2</sub>, CO, and NO on Surface Segregation in a Rh<sub>0.5</sub>Pd<sub>0.5</sub> Bulk Crystal and Comparison to Rh<sub>0.5</sub>Pd<sub>0.5</sub> Nanoparticles. *Langmuir* **2010**, *26*, 16362-16367.

18. Di Paola, C.; Baletto, F., Oxygen Adsorption on Small PtNi Nanoalloys. *Phys. Chem. Chem. Phys.* **2011**, *13*, 7701.
19. Mu, R.; Guo, X.; Fu, Q.; Bao, X., Oscillation of Surface Structure and Reactivity of PtNi Bimetallic Catalysts with Redox Treatments at Variable Temperatures. *J. Phys. Chem. C* **2011**, *115*, 20590–20595.
20. Austin, N.; Butina, B.; Mpourmpakis, G., CO<sub>2</sub> Activation on Bimetallic CuNi Nanoparticles. *Prog. Nat. Sci.* **2016**, *26*, 487–492.
21. Kitayama, Y.; Watanabe, Y.; Muramatsu, K.; Kodama, T., Catalytic Reduction of Carbon Dioxide on NiCu Alloys. *Energy* **1997**, *22*, 177–182.
22. Liu, Y.; Liu, D., Study of Bimetallic Cu–Ni/ $\gamma$ -Al<sub>2</sub>O<sub>3</sub> Catalysts for Carbon Dioxide Hydrogenation. *Int. J. Hydrogen Energy* **1999**, *24*, 351–354.
23. Nerlov, J.; Chorkendorff, I., Methanol Synthesis from CO<sub>2</sub>, CO, and H<sub>2</sub> over Cu(100) and Ni/Cu(100). *J. Catal.* **1999**, *181*, 271–279.
24. Studt, F.; Abild-Pedersen, F.; Wu, Q.; Jensen, A. D.; Temel, B.; Grunwaldt, J.-D.; Nørskov, J. K., CO Hydrogenation to Methanol on Cu–Ni Catalysts: Theory and Experiment. *J. Catal.* **2012**, *293*, 51–60.
25. Sinfelt, J. H., Catalytic Hydrogenolysis and Dehydrogenation over Copper-Nickel Alloys. *J. Catal.* **1972**, *24*, 283–296.
26. Modak, S.; Khanra, B. C., Studies on the Effect of Surface Segregation on Hydrocarbon Conversion over Cu-Ni Alloys. *Surf. Sci.* **1988**, *199*, 361–370.
27. Lortie, M.; Isaifan, R.; Liu, Y.; Mommers, S., Synthesis of CuNi/C and CuNi/ $\gamma$ -Al<sub>2</sub>O<sub>3</sub> Catalysts for the Reverse Water Gas Shift Reaction. *Int. J. Chem. Eng.* **2015**, *2015*, 1–9.
28. Chen, L.-C.; Lin, S. D., The Ethanol Steam Reforming over Cu-Ni/SiO<sub>2</sub> Catalysts: Effect of Cu/Ni Ratio. *Appl. Catal., B* **2011**, *106*, 639–649.
29. Chen, L.-C.; Lin, S. D., Effects of the Pretreatment of CuNi/SiO<sub>2</sub> on Ethanol Steam Reforming: Influence of Bimetal Morphology. *Appl. Catal., B* **2014**, *148-149*, 509–519.
30. Hornés, A.; Bera, P.; Fernández-García, M.; Guerrero-Ruiz, A.; Martínez-Arias, A., Catalytic and Redox Properties of Bimetallic Cu–Ni Systems Combined with CeO<sub>2</sub> or Gd-Doped CeO<sub>2</sub> for Methane Oxidation and Decomposition. *Appl. Catal., B* **2012**, *111-112*, 96–105.
31. Yang, Y.; White, M. G.; Liu, P., Theoretical Study of Methanol Synthesis from CO<sub>2</sub> Hydrogenation on Metal-Doped Cu(111) Surfaces. *J. Phys. Chem. C* **2012**, *116*, 248–256.
32. Vesselli, E., et al., Steering the Chemistry of Carbon Oxides on a NiCu Catalyst. *ACS Catal.* **2013**, *3*, 1555–1559.
33. Zhao, F.; Gong, M.; Cao, K.; Zhang, Y.; Li, J.; Chen, R., Atomic Layer Deposition of Ni on Cu Nanoparticles for Methanol Synthesis from CO<sub>2</sub> Hydrogenation. *ChemCatChem* **2017**, DOI: 10.1002/cctc.201700622.
34. Nerlov, J.; Chorkendorff, I., Promotion through Gas Phase Induced Surface Segregation: Methanol Synthesis from CO, CO<sub>2</sub> and H<sub>2</sub> over Ni/Cu(100). *Catal. Lett.* **1998**, *54*, 171–176.
35. Pauling, L., Atomic Radii and Interatomic Distances in Metals. *J. Am. Chem. Soc.* **1947**, *69*, 542–553.
36. Vitos, L.; Ruban, A. V.; Skriver, H. L.; Kollár, J., The Surface Energy of Metals. *Surf. Sci.* **1998**, *411*, 186–202.
37. Wei, Y.; Chen, S., Size-Dependent Surface Energy Density of Spherical Face-Centered-Cubic Metallic Nanoparticles. *J. Nanosci. Nanotechnol.* **2015**, *15*, 9457–9463.

38. Gaskell, D. R., *Introduction to the Thermodynamics of Materials*, 5th ed.; Taylor & Francis Group, LLC: New York, 2008.
39. Tsong, T. T.; Ng, Y. S.; McLane, S. B., Surface Segregation of NiCu Alloy in Nitrogen and Oxygen: An Atom Probe Field Ion Microscope Study. *J. Appl. Phys.* **1980**, *51*, 6189-6191.
40. Kamiya, I.; Hashizume, T.; Sakai, A.; Sakurai, T.; Pickering, H. W., Chemisorption-Induced Surface Segregation in Cu-Ni Alloys. *Le Journal de Physique Colloques* **1986**, *47*, C7-195-C7-201.
41. Montejano-Carrizales, J. M.; Morán-López, J. L., Oxygen Chemisorption Effects on the Spatial Atomic Distribution of CuNi, CuPd and NiPt Nanostructures. *Surf. Sci.* **1993**, *287-288*, 1070–1075.
42. Takasu, Y.; Shimizu, H.; Maru, S.-i.; Matsuda, Y., Auger Spectroscopic Study on the Surface Composition of CuNi Alloys Oxidized with Nitric Oxide. *Surf. Sci.* **1976**, *61*, 279-282.
43. Pike, J.; Chan, S.-W.; Zhang, F.; Wang, X.; Hanson, J., Formation of Stable Cu<sub>2</sub>O from Reduction of CuO Nanoparticles. *Appl. Catal., A* **2006**, *303*, 273-277.
44. Wang, Z.; You, Y.; Yuan, J.; Yin, Y.-X.; Li, Y.-T.; Xin, S.; Zhang, D., Nickel-Doped La<sub>0.8</sub>Sr<sub>0.2</sub>Mn<sub>1-x</sub>Ni<sub>x</sub>O<sub>3</sub> Nanoparticles Containing Abundant Oxygen Vacancies as an Optimized Bifunctional Catalyst for Oxygen Cathode in Rechargeable Lithium–Air Batteries. *ACS Appl. Mater. Interfaces* **2016**, *8*, 6520-6528.
45. Beaumont, S. K.; Alayoglu, S.; Pushkarev, V. V.; Liu, Z.; Kruse, N.; Somorjai, G. A., Exploring Surface Science and Restructuring in Reactive Atmospheres of Colloidally Prepared Bimetallic CuNi and CuCo Nanoparticles on SiO<sub>2</sub> in situ Using Ambient Pressure X-Ray Photoelectron Spectroscopy. *Faraday Discuss.* **2013**, *162*, 31.
46. Modak, S.; Khanra, B. C., Surface Segregation in the Hydrogen-Adsorbed Cu-Ni Alloy. *Phys. Rev. B* **1986**, *34*, 5909–5911.
47. Luo, J.; Maye, M. M.; Petkov, V.; Kariuki, N. N.; Wang, L.; Njoki, P.; Mott, D.; Lin, Y.; Zhong, C.-J., Phase Properties of Carbon-Supported Gold–Platinum Nanoparticles with Different Bimetallic Compositions. *Chem. Mater.* **2005**, *17*, 3086–3091.
48. Kitla, A.; Safonova, O. V.; Föttinger, K., Infrared Studies on Bimetallic Copper/Nickel Catalysts Supported on Zirconia and Ceria/Zirconia. *Catal. Lett.* **2013**, *143*, 517-530.
49. Ahmadi, M.; Behafarid, F.; Cui, C.; Strasser, P.; Roldan Cuenya, B., Long-Range Segregation Phenomena in Shape-Selected Bimetallic Nanoparticles: Chemical State Effects. *ACS Nano* **2013**, *7*, 9195-9204.
50. van den Oetelaar, L. C. A.; Partridge, A.; Toussaint, S. L. G.; Flipse, C. F. J.; Brongersma, H. H., A Surface Science Study of Model Catalysts. 2. Metal–Support Interactions in Cu/SiO<sub>2</sub> Model Catalysts. *J. Phys. Chem. B* **1998**, *102*, 9541-9549.
51. Divins, N. J.; Angurell, I.; Escudero, C.; Pérez-Dieste, V.; Llorca, J., Influence of the Support on Surface Rearrangements of Bimetallic Nanoparticles in Real Catalysts. *Science* **2014**, *346*, 620–623.
52. Ono, L. K.; Behafarid, F.; Roldan Cuenya, B., Nano-Gold Diggers: Au-Assisted SiO<sub>2</sub>-Decomposition and Desorption in Supported Nanocatalysts. *ACS Nano* **2013**, *7*, 10327-10334.
53. Ahmadi, M.; Mistry, H.; Roldan Cuenya, B., Tailoring the Catalytic Properties of Metal Nanoparticles Via Support Interactions. *J. Phys. Chem. Lett.* **2016**, *7*, 3519-3533.
54. Jak, M. J. J.; Konstapel, C.; Van Kreuningen, A.; Chrost, J.; Verhoeven, J.; Frenken, J. W. M., The Influence of Substrate Defects on the Growth Rate of Palladium Nanoparticles on a TiO<sub>2</sub>(110) Surface. *Surf. Sci.* **2001**, *474*, 28.

55. Naitabdi, A.; Roldan Cuenya, B., Formation, Thermal Stability and Surface Composition of Size-Selected AuFe Nanoparticles. *Appl. Phys. Lett.* **2007**, *91*, 113110.
56. Porsgaard, S.; Merte, L. R.; Ono, L. K.; Behafarid, F.; Matos, J.; Helveg, S.; Salmeron, M.; Roldan Cuenya, B.; Besenbacher, F., Stability of Platinum Nanoparticles Supported on SiO<sub>2</sub>/Si(111): A High-Pressure X-Ray Photoelectron Spectroscopy Study. *ACS nano* **2012**, *6*, 10743-10749.
57. C.D. Wagner, A. V. N., A. Kraut-Vass, J.W. Allison, C.J. Powell, J.R.Jr. Rumble, NIST Standard Reference Database 20, version 3.4 (web version) (<http://srdata.nist.gov/xps/>) **2003**.
58. Biesinger, M. C.; Lau, L. W. M.; Gerson, A. R.; Smart, R. S. C., Resolving Surface Chemical States in XPS Analysis of First Row Transition Metals, Oxides and Hydroxides: Sc, Ti, V, Cu and Zn. *Appl. Surf. Sci.* **2010**, *257*, 887–898.
59. Speckmann, H. D.; Haupt, S.; Strehblow, H.-H., A Quantitative Surface Analytical Study of Electrochemically-Formed Copper Oxides by XPS and X-Ray-Induced Auger Spectroscopy. *Surf. Interface Anal.* **1988**, *11*, 148–155.
60. Wu, C.-K.; Yin, M.; O'Brien, S.; Koberstein, J. T., Quantitative Analysis of Copper Oxide Nanoparticle Composition and Structure by X-Ray Photoelectron Spectroscopy. *Chem. Mater.* **2006**, *18*, 6054–6058.
61. Hirsimäki, M.; Lampimäki, M.; Lahtonen, K.; Chorkendorff, I.; Valden, M., Investigation of the Role of Oxygen Induced Segregation of Cu During Cu<sub>2</sub>O Formation on Cu{100}, Ag/Cu{100} and Cu(Ag) Alloy. *Surf. Sci.* **2005**, *583*, 157–165.
62. McIntyre, N. S.; Sunder, S.; Shoesmith, D. W.; Stanchell, F. W., Chemical Information from XPS—Applications to the Analysis of Electrode Surfaces. *J. Vac. Sci. Technol.* **1981**, *18*, 714-721.
63. Biesinger, M. C.; Payne, B. P.; Lau, L. W. M.; Gerson, A.; Smart, R. S. C., X-Ray Photoelectron Spectroscopic Chemical State Quantification of Mixed Nickel Metal, Oxide and Hydroxide Systems. *Surf. Interface Anal.* **2009**, *41*, 324-332.
64. Grosvenor, A. P.; Biesinger, M. C.; Smart, R. S. C.; McIntyre, N. S., New Interpretations of XPS Spectra of Nickel Metal and Oxides. *Surf. Sci.* **2006**, *600*, 1771–1779.
65. Biesinger, M. C.; Payne, B. P.; Grosvenor, A. P.; Lau, L. W. M.; Gerson, A. R.; Smart, R. S. C., Resolving Surface Chemical States in XPS Analysis of First Row Transition Metals, Oxides and Hydroxides: Cr, Mn, Fe, Co and Ni. *Appl. Surf. Sci.* **2011**, *257*, 2717–2730.
66. Kim, K. S.; Winograd, N., X-Ray Photoelectron Spectroscopic Studies of Nickel-Oxygen Surfaces Using Oxygen and Argon Ion-Bombardment. *Surf. Sci.* **1974**, *43*, 625–643.
67. Carley, A. F.; Jackson, S. D.; O'Shea, J. N.; Roberts, M. W., The Formation and Characterisation of Ni<sup>3+</sup> — an X-Ray Photoelectron Spectroscopic Investigation of Potassium-Doped Ni(110)–O. *Surf. Sci.* **1999**, *440*, L868-L874.
68. Mansour, A. N., Characterization of NiO by XPS. *Surf. Sci. Spectra* **1994**, *3*, 231.
69. Barbieri, P. F.; Siervo, A. d.; Carazzolle, M. F.; Landers, R.; Kleiman, G. G., XPS and XAES Study of Ag–Pd and Cu–Ni Alloys: Spectra, Shifts and Electronic Structure Information. *J. Electron. Spectrosc. Relat. Phenom.* **2004**, *135*, 113–118.
70. Webber, P. R.; Rojas, C. E.; Dobson, P. J.; Chadwick, D., A Combined XPS/AES Study of Cu Segregation to the High and Low Index Surfaces of a Cu-Ni Alloy. *Surf. Sci.* **1981**, *105*, 20–40.